Thioesterase superfamily member 2 promotes hepatic insulin resistance in the setting of glycerol-3-phosphate acyltransferase 1–induced steatosis

Received for publication, August 2, 2018, and in revised form, November 21, 2018 Published, Papers in Press, December 6, 2018, DOI 10.1074/jbc.RA118.005184

Veronika Tillander[‡§], Akihiro Miniami[‡¶], Michele Alves-Bezerra[‡1], Rosalind A. Coleman[‖], and David E. Cohen[‡2]

From the [‡]Joan and Sanford I. Weill Department of Medicine, Weill Cornell Medical College, New York, New York 10021, the [§]Division of Clinical Chemistry, Department of Laboratory Medicine, Karolinska Institute, 14152 Huddinge, Sweden, the [¶]Department of Gastroenterology, Kobe University Graduate School of Medicine, Kobe 650-0017, Japan, and the [‖]Department of Nutrition, University of North Carolina, Chapel Hill, North Carolina 27599

Edited by Jeffrey E. Pessin

Hepatic insulin resistance in the setting of steatosis is attributable at least in part to the accumulation of bioactive lipids that suppress insulin signaling. The mitochondria-associated glycerol-3-phosphate acyltransferase 1 (GPAT1) catalyzes the first committed step in glycerolipid synthesis, and its activity diverts fatty acids from mitochondrial β-oxidation. GPAT1 overexpression in mouse liver leads to hepatic steatosis even in the absence of overnutrition. The mice develop insulin resistance owing to the generation of saturated diacylglycerol and phosphatidic acid molecular species that reduce insulin signaling by activating PKCε and by suppressing mTORC2, respectively. Them2, a mitochondria-associated acyl-CoA thioesterase, also participates in the trafficking of fatty acids into oxidative *versus* glycerolipid biosynthetic pathways. *Them2*$^{-/-}$ mice are protected against diet-induced hepatic steatosis and insulin resistance. To determine whether Them2 contributes to hepatic insulin resistance due to hepatic overexpression of GPAT1, recombinant adenovirus was used to overexpress GPAT1 in livers of chow-fed *Them2*$^{+/+}$ and *Them2*$^{-/-}$ mice. Hepatic GPAT1 overexpression led to steatosis in both genotypes. In the setting of GPAT1 overexpression, glucose tolerance was reduced in *Them2*$^{+/+}$ but not *Them2*$^{-/-}$ mice, without influencing whole-body insulin sensitivity or basal hepatic glucose production. Improved glucose tolerance in *Them2*$^{-/-}$ mice was associated with reduced PKCε translocation. Preserved insulin receptor activity was supported by Thr-308 phosphorylation of Akt following GPAT1 overexpression in *Them2*$^{-/-}$ hepatocytes. These findings suggest a pathogenic role of Them2 in the biosynthesis of glycerolipid metabolites that promote hepatic insulin resistance.

This work was supported by NIDDK, National Institutes of Health, Grants R37 DK048873 and R01 DK056626 (to D. E. C.) and R01 DK56598 (to R. A. C.), the Swedish Society for Medical Research (SSMF) Postdoctoral Research Fellowship 201525 (to V.T.), and American Heart Association Postdoctoral Fellowship 18POST33990445 (to M. A.-B.). The authors declare that they have no conflicts of interest with the contents of this article. The content is solely the responsibility of the authors and does not necessarily represent the official views of the National Institutes of Health.

[1] Recipient of an American Liver Foundation NASH Fatty Liver Disease Postdoctoral Research Fellowship Award.

[2] To whom correspondence should be addressed: Belfer Research Bldg., 413 E. 69th St., Rm. 630, New York, NY 10021. Tel.: 646-962-7681; Fax: 646-962-0427; E-mail: dcohen@med.cornell.edu.

Nonalcoholic fatty liver disease (NAFLD)[3] has emerged as a global epidemic, with a world-wide prevalence of ~25% (1). Common comorbidities include obesity, metabolic syndrome, and type 2 diabetes. Lipid accumulation within the liver is closely associated with the development of hepatic insulin resistance. Although the mechanisms are not fully understood, bioactive lipid species play key roles in suppressing insulin signaling. These include free fatty acids (FFA) and the glycerolipids diacylglycerols (DAG) and phosphatidic acids (PA) (2).

Glycerol-3-phosphate acyltransferase (GPAT) catalyzes the initial committed step in glycerolipid biosynthesis. Current concepts suggest that the activity of GPAT isoform 1 (GPAT1), which is located at the mitochondrial outer membrane, is a key determinant of fatty acid trafficking between glycerolipid synthesis and mitochondrial β-oxidation (3). Overexpression of GPAT1 in liver and isolated hepatocytes causes increased triacylglycerol (TAG) synthesis, with a reciprocal decrease in mitochondrial β-oxidation, indicative of competition with carnitine palmitoyltransferase 1a (CPT1a) for newly esterified fatty acyl-CoAs at the mitochondrial outer membrane (4–6). Conversely, the absence of GPAT1 results in reduced TAG synthesis and an increase in fatty acid oxidation and ketogenesis (7). GPAT1-induced lipid accumulation leads to decreased insulin signaling and reduced hepatic glucose tolerance, which are attributable to the hepatocellular accumulation of DAG and PA (6, 8–10). In keeping with this observation, mice lacking GPAT1 (*Gpat1*$^{-/-}$) are protected against hepatic steatosis and insulin resistance (11).

Thioesterase superfamily member 2 (Them2; synonym acyl-CoA thioesterase (ACOT) 13) is a mitochondria-associated long-chain ACOT that is enriched in oxidative tissues, including liver (12, 13). Them2 functions in the trafficking of long-chain fatty acids into oxidative *versus* glycerolipid biosynthetic

[3] The abbreviations used are: NAFLD, nonalcoholic fatty liver disease; ANCOVA, analysis of covariance; AUC, area under the curve; ACS, acyl-CoA synthetase; DAG, diacylglycerol; CPT, carnitine palmitoyltransferase; ER, endoplasmic reticulum; FFA, free fatty acid(s); GPAT1, glycerol-3-phosphate acyltransferase 1; PA, phosphatidic acid; TAG, triacylglycerol; ACOT, acyl-CoA thioesterase; ITT, insulin tolerance test; GTT, glucose tolerance test; PTT, pyruvate tolerance test; PKC, protein kinase C; mTOR, mammalian target of rapamycin; NEM, *N*-ethylmaleimide; DTNB, 5,5′-dithiobis(2-nitrobenzoic acid); ALT, alanine aminotransferase; AST, aspartate aminotransferase; PC-TP, phosphatidylcholine transfer protein.

pathways (14). Under fasting conditions in cultured mouse hepatocytes, Them2 promotes fatty acid oxidation (15). In contrast, under conditions of overnutrition either *in vivo* or in cell culture, Them2, instead, promotes the incorporation of saturated fatty acids into ER membrane phospholipids, leading to reduced ER membrane fluidity and increased calcium efflux and to activation of ER stress pathways and gluconeogenesis (16). When taken together, the data suggest that Them2 preferentially hydrolyzes long-chain fatty acyl-CoAs, which then become the substrate for a mitochondria-associated fatty acyl-CoA synthetase (ACS) isoform. Depending upon nutritional status, ACS can supply newly formed long-chain acyl-CoA either to CPT1a for mitochondrial uptake and β-oxidation or to GPAT1 for glycerolipid biosynthesis. Like *Gpat1*$^{-/-}$ mice, *Them2*$^{-/-}$ mice exhibit improved glucose homeostasis and are resistant to diet-induced hepatic insulin resistance and steatosis (17).

To test whether Them2 may also function upstream of GPAT1 to provide fatty acids for incorporation into bioactive glycerolipid molecular species that suppress insulin signaling, we utilized recombinant adenovirus to overexpress GPAT1 in livers and hepatocytes of *Them2*$^{-/-}$ mice and their respective controls. Although hepatic GPAT1 overexpression promoted hepatic steatosis irrespective of Them2 expression, the absence of Them2 expression improved glucose tolerance in a manner consistent with decreased DAG-mediated suppression of hepatic insulin signaling.

Results

No effect of liver-specific overexpression of GPAT1 on body or liver weights

Ad-GPAT1 infection–induced overexpression of GPAT1 was liver-specific, as evidenced by detection of the FLAG tag and increased GPAT1 expression levels along with vector-specific GFP in liver, but not in other tissues (Fig. 1*A*). Ad-GPAT1 administration increased GPAT1 protein by 3.9- and 6.5-fold in *Them2*$^{+/+}$ and *Them2*$^{-/-}$, respectively, compared with Ad-GFP infected controls (Fig. 1*B*). Accordingly, *Gpat1* mRNA levels were 7.5- and 7.6-fold higher in livers of *Them2*$^{+/+}$ and *Them2*$^{-/-}$ mice administered Ad-GPAT1 relative to controls (Fig. 1*C*). Following GPAT1 overexpression, total GPAT activity was higher in livers of both genotypes compared with controls (Fig. 1*D*). This difference was attributable primarily to 2.3- and 1.8-fold increases in *N*-ethylmaleimide (NEM)-resistant GPAT activity (GPAT1) in *Them2*$^{+/+}$ and *Them2*$^{-/-}$ mice, respectively (Fig. 1*D*) (18, 19). The absence of genotype-related differences before or after overexpression demonstrates that Them2 expression *per se* did not influence the activity of GPAT1. The hepatic overexpression of GPAT1 did not influence body weight (Fig. 1*E*), liver weight (Fig. 1*F*), or the percentages of lean or fat mass (Fig. 1*G*). Percentages of fat were slightly higher in *Them2*$^{-/-}$ mice, but this did not achieve statistical significance among the different groups (Fig. 1*G*).

Neither Them2 protein (Fig. 1*A*) nor mRNA (Fig. 1*H*) levels were influenced by the overexpression of GPAT1. The acyl-CoA thioesterase activity of liver homogenates was largely unaffected by GPAT1 expression or genotype (Fig. 1*I*), presumably because of the presence of other ACOT isoforms in liver (14). After GPAT1 overexpression, no changes were detected in the apparent V_{max}, but the apparent K_m in *Them2*$^{+/+}$ mice was lower compared with control (Fig. 1, *I* and *J*). In keeping with minor changes in ACOT activity, there were no significant changes in the mRNA expression of the other liver-enriched ACOT isoforms, either in cytosol (*Acot1* and *-7*) or mitochondria (*Acot2*) (Fig. 1*K*); these ACOT isoforms all also share overlapping substrate specificities with Them2 (14).

GPAT1 overexpression induces hepatic steatosis irrespective of Them2 expression

GPAT1 overexpression increased hepatic TAG concentrations in both *Them2*$^{+/+}$ and *Them2*$^{-/-}$ mice (Fig. 2*A*). Although the absolute TAG concentrations were higher in *Them2*$^{-/-}$ mice following GPAT1 overexpression, the -fold increase was greater in *Them2*$^{+/+}$ mice (8.2-fold) compared with *Them2*$^{-/-}$ mice (5.7-fold) (Fig. 2*A*). Increases in TAG concentrations were affirmed by histology (Fig. 2*C*), which revealed microvesicular steatosis following hepatic GPAT1 overexpression in both genotypes. Hepatic concentrations of phospholipids (Fig. 2*B*) and FFA (Fig. 2*D*) tended to increase in response to GPAT1 overexpression in both genotypes, with a reciprocal decrease of plasma levels of FFA that achieved significance in *Them2*$^{-/-}$ mice following GPAT1 overexpression (Fig. 2*E*). No change was observed in hepatic cholesterol concentrations (data not shown).

The mRNA expression of *Acsl1* was not affected by the GPAT1 overexpression (Fig. 2*F*). Decreased expression of genes encoding key lipogenic enzymes in response to GPAT1 overexpression was observed: *Fasn* and *Dgat1* were down-regulated in *Them2*$^{-/-}$ mice, with a similar trend observed for *Acaca* and for *Gpat4* (Fig. 2*F*). Additionally, compared with *Them2*$^{+/+}$ mice, *Agpat1* and *Agpat2* also decreased upon GPAT1 overexpression, with decreases also noted for *Agpat1* and *2* in livers of *Them2*$^{-/-}$ mice (Fig. 2*F*). The expression of *Cpt1a* was higher in *Them2*$^{-/-}$ mice compared with *Them2*$^{+/+}$ mice in the setting of GPAT1 overexpression, and the expression of the Them2-interacting protein *Pctp* tended to be lower under the same conditions (Fig. 2*F*).

Plasma lipid concentrations were not influenced by GPAT1 overexpression (Fig. 2, *G–I*) with the exception of a modest increase in cholesterol in *Them2*$^{+/+}$ mice (Fig. 2*I*). Following Ad-GFP administration, plasma activities of both aspartate aminotransferase (AST) (Fig. 2*J*) and alanine aminotransferase (ALT) (Fig. 2*K*) were greater in the absence of Them2 expression. However, this difference was not observed in response to the overexpression of GPAT1, which significantly decreased the plasma activities of both AST and ALT in *Them2*$^{-/-}$ mice. Notwithstanding, mRNA expression of ER stress–related genes *Xbp1*, *Chop*, and *Aft6* was unaffected by GPAT1 expression or genotype (Fig. 2*L*). Although previous experience revealed no influence of control or GPAT1 adenovirus on inflammatory markers under similar experimental conditions (8), we investigated whether these were associated with evidence of hepatic inflammation in the current study. There were no differences in mRNA expression of inflammatory genes observed among the groups (Fig. 2*L*). This is in line with the absence of histologic evidence of injury or inflammation in response to GPAT1 over-

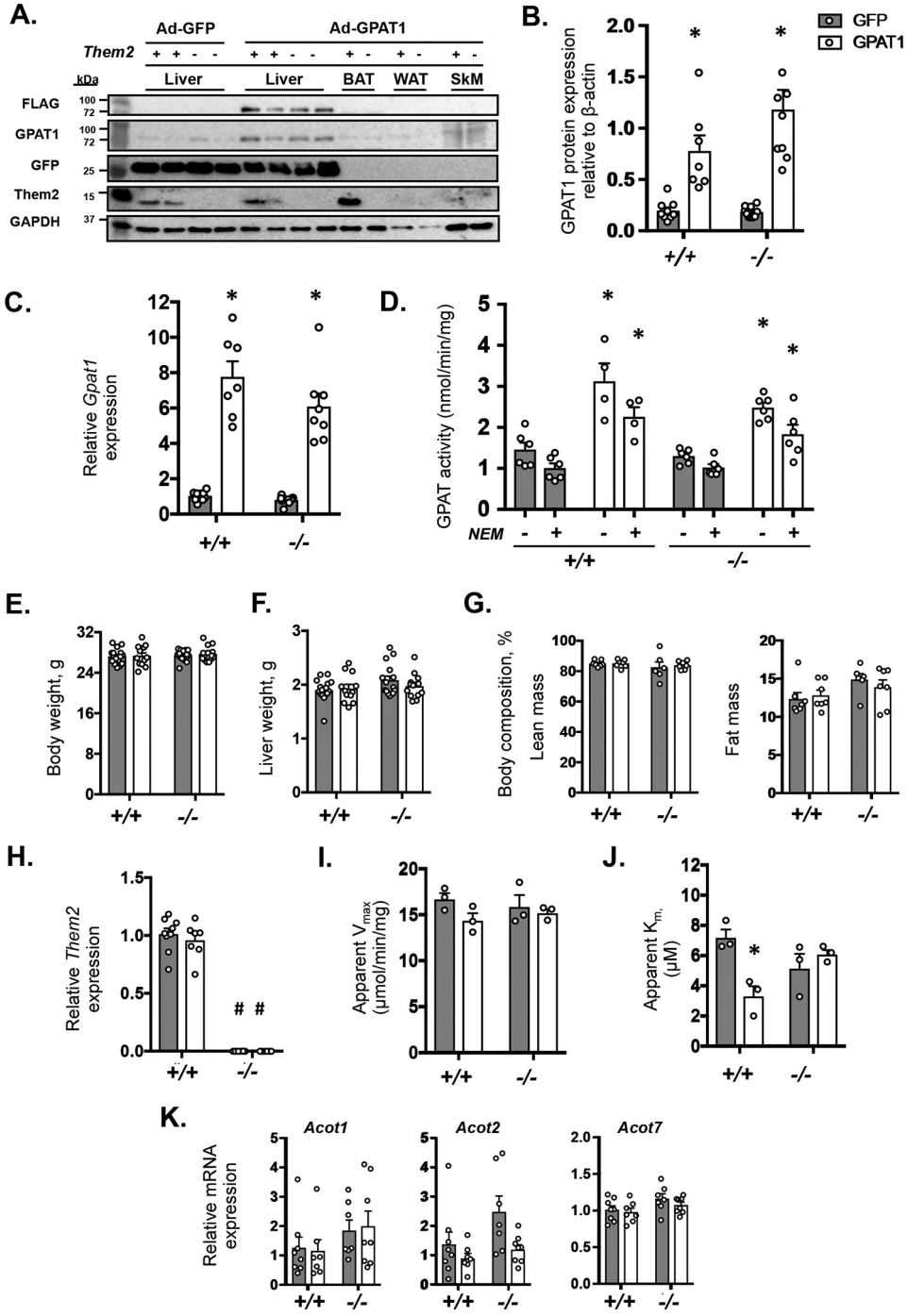

Figure 1. Adenovirus-mediated overexpression of GPAT1 in livers of *Them2*$^{+/+}$ and *Them2*$^{-/-}$ mice. Hepatic overexpression of GPAT1 was demonstrated 12 days following administration of Ad-GPAT1-sequence adenoviral vector relative to control Ad-GFP (n = 7–10/group) by immunoblot analyses demonstrating that GPAT1 expression is restricted to the liver (*A*), densitometric analysis of GPAT1 expression (*B*), and mRNA expression of *Gpat1* (*C*). *D*, GPAT activity was determined in the absence (−) or presence (+) of NEM, which yields total and GPAT1-specific activities, respectively (n = 4–6/group). *E*, body weights; *F*, liver weights; *G*, body compositions of adenovirus-treated mice (n = 7–10/group). *H*, mRNA expression of *Them2* following adenovirus infection (n = 7–10/group). Values are relative to expression in *Them2*$^{+/+}$ Ad-GFP. Steady-state values for fatty acyl-CoA thioesterase activity of apparent V_{max} (*I*) and apparent K_m (*J*) were determined in liver homogenates (n = 3/group). *K*, influence of GPAT1 overexpression on the hepatic mRNA expression of *Acot1*, *Acot2*, and *Acot7* (n = 7–10/group). Values represent mean ± S.E. (*error bars*). Differences were detected by post hoc testing following two-way ANOVA. *, $p < 0.05$, GFP *versus* GPAT1; #, $p < 0.05$, *Them2*$^{+/+}$ *versus* *Them2*$^{-/-}$.

expression (Fig. 2*C*). Because esterification of fatty acids into triglycerides can be hepatoprotective, as has been described in the literature on nonalcoholic fatty liver disease (20), the elevations in transaminases may reflect the compartmentalized elevations in intracellular free fatty acids that were not apparent by biochemical measurements of homogenized livers.

Improved glucose tolerance and hepatic insulin signaling after GPAT1 overexpression in the absence of Them2

Hepatic GPAT1 overexpression did not affect baseline glucose concentrations in either *Them2*$^{+/+}$ or *Them2*$^{-/-}$ mice (time 0 values in Fig. 3*A*). However, during the glucose tolerance tests (GTTs) in *Them2*$^{+/+}$ mice, GPAT1 overexpression

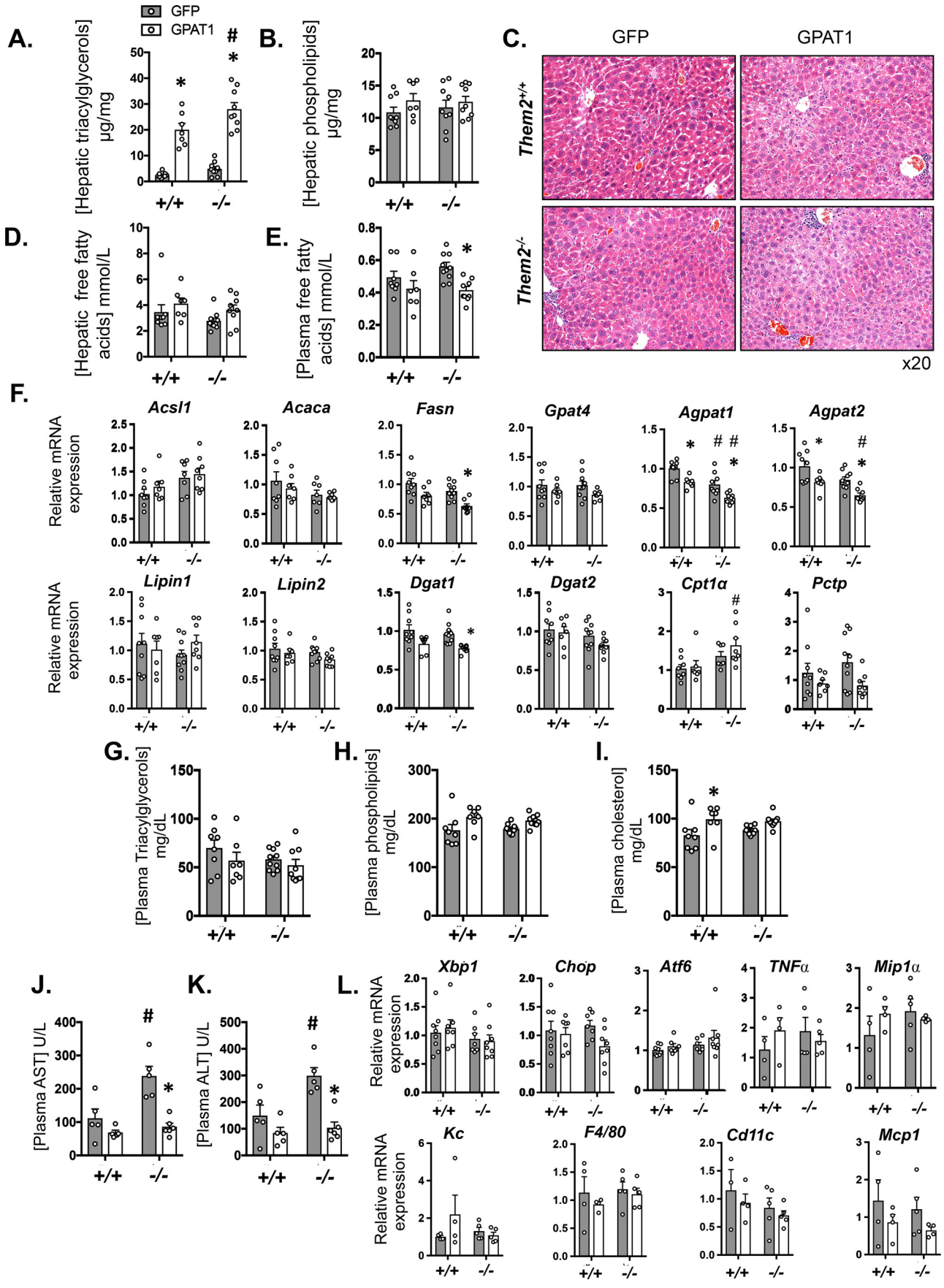
A.
GFP
GPAT1
[Hepatic triacylglycerols] µg/mg
B.
[Hepatic phospholipids] µg/mg
C.
GFP
GPAT1
Them2+/+
Them2-/-
x20
D.
[Hepatic free fatty acids] mmol/L
E.
[Plasma free fatty acids] mmol/L
F.
Acsl1
Acaca
Fasn
Gpat4
Agpat1
Agpat2
Lipin1
Lipin2
Dgat1
Dgat2
Cpt1α
Pctp
Relative mRNA expression
G.
[Plasma Triacylglycerols] mg/dL
H.
[Plasma phospholipids] mg/dL
I.
[Plasma cholesterol] mg/dL
J.
[Plasma AST] U/L
K.
[Plasma ALT] U/L
L.
Xbp1
Chop
Atf6
TNFα
Mip1α
Kc
F4/80
Cd11c
Mcp1
+/+
-/-

resulted in higher plasma glucose concentrations with increased AUC values (Fig. 3*A*). This was not observed in *Them2*$^{-/-}$ mice, in which GPAT1 overexpression increased neither time-dependent plasma glucose concentrations nor AUC values (Fig. 3*A*). Insulin tolerance tests (ITTs) revealed no difference due to hepatic GPAT1 overexpression in *Them2*$^{+/+}$ mice (Fig. 3*B*). The modest increase in endogenous glucose clearance in *Them2*$^{-/-}$ mice only achieved significance at one single time point, and there were no differences in AUC values (Fig. 3*B*). During pyruvate tolerance tests (PTTs), GPAT1 overexpression did not influence blood glucose concentrations at any time point for either genotype; nor were differences observed in the AUC values (Fig. 3*C*). These PTT results are in keeping with previously published clamp experiments on mice transduced with the same adenovirus under similar conditions (8), which demonstrated that basal hepatic glucose production is not affected by GPAT1 overexpression.

Two key transcriptional mediators of insulin signaling and glucose homeostasis, *Foxo1* and *Chrebpα*, and selected target genes were investigated (Fig. 3*C*). Decreases in *Foxo1* and its target genes phosphoenolpyruvate carboxykinase (*Pepck*) and glucose-6-phosphatase (*G6p*), in the absence of Them2 expression were not significant (Fig. 3*C*). *Chrebpα* was differentially regulated by GPAT1 overexpression in the two genotypes, with a reduced expression in *Them2*$^{-/-}$ mice following GPAT1 overexpression compared with GPAT1-overexpressing *Them2*$^{+/+}$ mice (Fig. 3*C*). Decreases in mRNA expression of the target gene pyruvate kinase (*Pklr*) in response to GPAT1 overexpression and to Them2 ablation were not significant (Fig. 3*C*).

Overexpression of GPAT1 induces hepatic insulin resistance due to the biosynthesis of excess DAG and PA, which activate PKCε and suppress mTORC2 activity, respectively (8, 10). A metric of PKCε activation is its translocation to the plasma membrane (8, 10). DAG promote translocation, where activated PKCε reduces insulin receptor kinase activity by phosphorylation at Thr-1160, thereby suppressing the insulin signaling cascade, including the phosphorylation of Akt at Thr-308 (21). GPAT1 overexpression increased membrane translocation of PKCε in *Them2*$^{+/+}$ but not *Them2*$^{-/-}$ mice (Fig. 3*E*). In keeping with its effects on hepatic TAG concentrations (Fig. 2*A*), GPAT1 overexpression increased hepatic DAG concentrations by 2.9- and 3.2-fold in *Them2*$^{+/+}$ and *Them2*$^{-/-}$ mice, respectively (Fig. 3*F*). However, in the setting of GPAT1 overexpression in *Them2*$^{-/-}$ mice, there was a trend toward a reduction in the proportions of DAG containing saturated fatty acids (Fig. 3*F*), which are consistently elevated in the setting of PKCε activation (22). Because mTORC2-mediated phosphorylation of Akt at Ser-473 is required for its full activation, PA-mediated inhibition of mTORC2 activity is a second potential mechanism of hepatic insulin resistance in response to GPAT1 overexpression. However, we did not observe differences in mTORC2 activity in hepatic tissue lysates in response to GPAT1 overexpression in either genotype (data not shown).

Selective reduction of Akt phosphorylation at Thr-308 following GPAT1 overexpression in Them2$^{+/+}$ *hepatocytes*

We first investigated the effect on GPAT1 overexpression on insulin signaling *in vivo* in experiments in which fasted mice were injected with a supraphysiological dose of insulin 10 min prior to sacrifice to maximize the phosphorylation of signaling proteins. Although insulin administration increased phosphorylation of IRS and Akt at both Thr-308 and Ser-473 in all groups (Fig. 4*A*), no differences were observed among genotypes in response to GPAT1 overexpression (Fig. 4, *A* and *B*). To assess these signaling events at a more physiological insulin concentration of 10 nM, we used primary hepatocytes from *Them2*$^{+/+}$ and *Them2*$^{-/-}$ mice. Following adenovirus infection *in vitro*, increased expression of GPAT1 was confirmed by the detection of the FLAG tag (Fig. 4, *C* and *D*) and activity of GPAT1 (Fig. 4*D*), which was similarly increased in both genotypes. In Ad-GFP–infected control hepatocytes, treatment with insulin increased Akt phosphorylation in both genotypes at both Thr-308 and Ser-473 (Fig. 4*C*). When Them2 was present, GPAT1 overexpression reduced phosphorylation of Akt at Thr-308 in response to 10 nM but not 100 nM insulin, whereas phosphorylation of Thr-308 was maintained in the absence of Them2 (Fig. 4*E*). In contrast, the expression of Them2 did not influence Ser-473 phosphorylation after GPAT1 overexpression.

Discussion

The principal findings of this study are that, in the setting of hepatic GPAT1 overexpression, Them2 1) does not influence TAG accumulation in the liver, 2) reduces glucose tolerance in the absence of changes in insulin tolerance, 3) increases the membrane translocation of PKCε, and 4) suppresses insulin-mediated Thr-308 phosphorylation of Akt. When taken together with studies of its role in hepatocellular lipid metabolism both *in vivo* and *in vitro* (15–17), these findings support a model (Fig. 5) in which Them2 regulates glucose homeostasis by channeling selected fatty acids into the glycerolipid synthetic pathway (14).

Whole-body *Them2*$^{-/-}$ mice are protected against high-fat diet–induced hepatic insulin resistance and steatosis (17). However, because these mice exhibit increased adaptive thermogenesis (23), the precise mechanistic contribution of hepatic Them2 to hepatic lipid and glucose metabolism remains unclear. Studies in cell culture systems support key roles for Them2 both in the hepatocellular trafficking of fatty acids and in insulin signaling. We previously provided evidence that mitochondria-associated Them2 participates in the selection of fatty acids for β-oxidation and glycerolipid synthesis and have suggested that the relative substrate specificity of Them2 for

Figure 2. Liver-specific GPAT1 overexpression promotes steatosis irrespective of Them2 expression. *A* and *B*, hepatic concentrations of TAG (*A*) and phospholipids (*B*) (n = 7–10/group). *C*, representative hematoxylin and eosin–stained liver sections from adenovirus-treated mice. *D* and *E*, free fatty acid concentrations in liver (*D*) and plasma (*E*). *F*, mRNA expression of selected genes in liver that regulate lipogenesis, triacylglycerol synthesis, and fatty acid oxidation (n = 7–10/group). Values are relative to expression in *Them2*$^{+/+}$ Ad-GFP. *G–I*, plasma concentrations of triacylglycerols (*G*), phospholipids (*H*), and cholesterol (*I*) (n = 7–10/group). *J* and *K*, plasma activities of AST (*J*) and ALT (*K*) (n = 5–6/group). *L*, mRNA expression of ER stress–related genes (n = 7–10/group) and inflammatory genes (n = 4–5/group) in liver. Values represent mean ± S.E. (*error bars*) Differences were detected by post hoc testing following two-way ANOVA. *, $p < 0.05$, GFP *versus* GPAT1; #, $p < 0.05$, *Them2*$^{+/+}$ *versus Them2*$^{-/-}$.

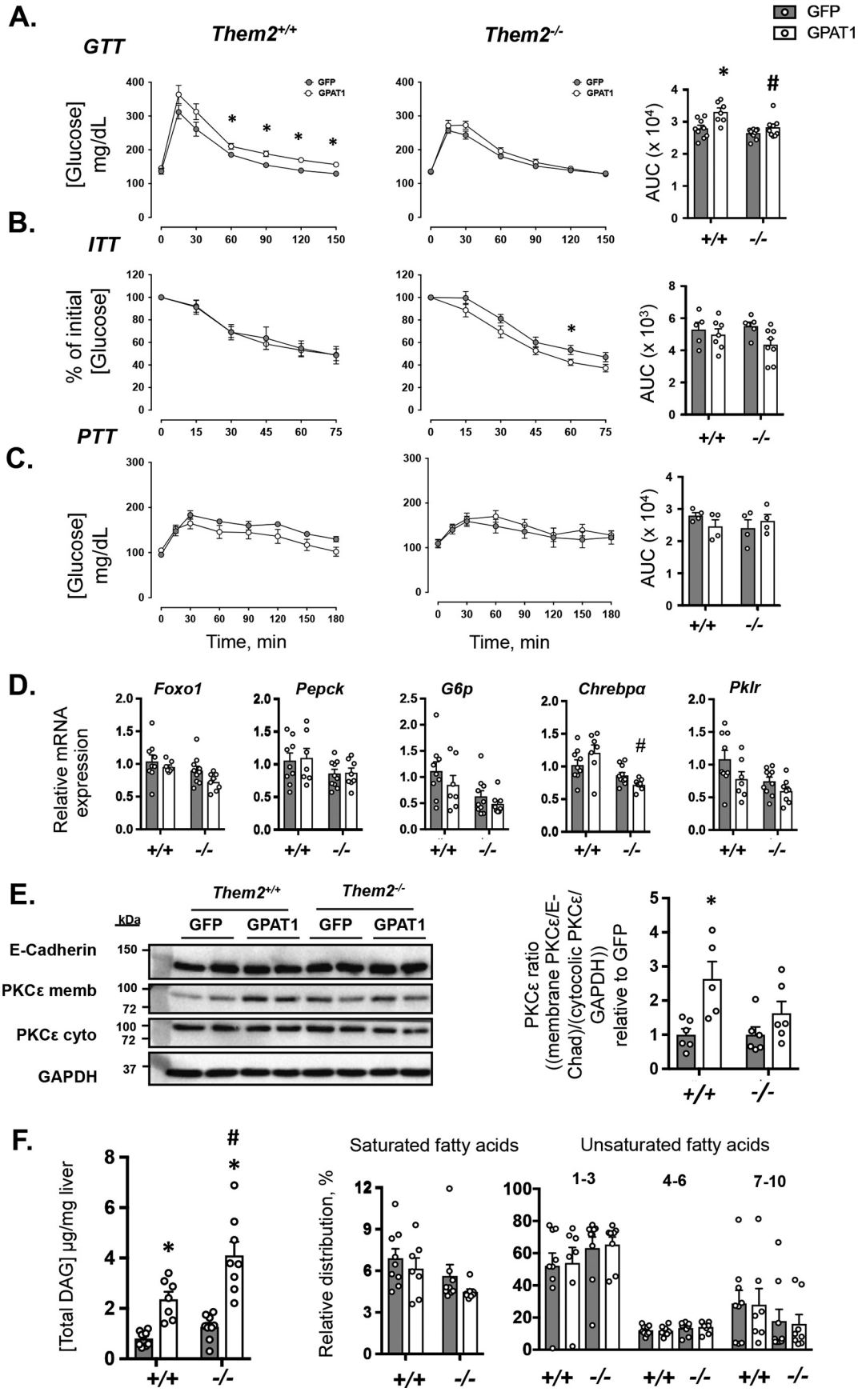
A.
GTT
Them2+/+
Them2-/-
GFP
GPAT1
[Glucose] mg/dL
AUC (x 10⁴)
+/+
-/-
B.
ITT
% of initial [Glucose]
AUC (x 10³)
C.
PTT
[Glucose] mg/dL
AUC (x 10⁴)
Time, min
D.
Foxo1
Pepck
G6p
Chrebpα
Pklr
Relative mRNA expression
E.
kDa
E-Cadherin
PKCε memb
PKCε cyto
GAPDH
PKCε ratio ((membrane PKCε/E-Chad)/(cytocolic PKCε/GAPDH)) relative to GFP
F.
[Total DAG] µg/mg liver
Saturated fatty acids
Unsaturated fatty acids
Relative distribution, %
1-3
4-6
7-10

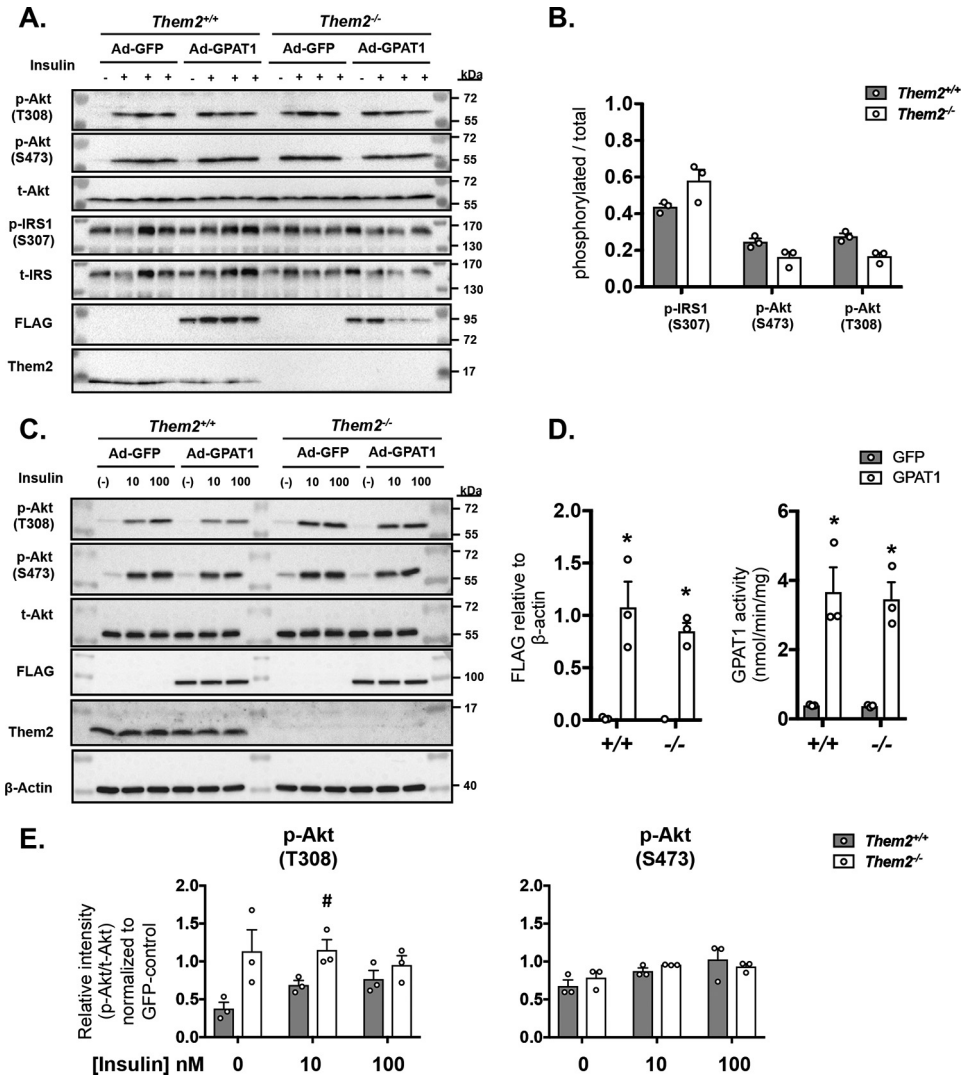

Figure 4. Ablation of Them2 protects against GPAT1-mediated reductions in insulin sensitivity. *A*, immunoblots to assess the phosphorylation of IRS and Akt 10 min following the intraperitoneal insulin administration (+) or PBS control (−) in livers from *Them2*$^{+/+}$ and *Them2*$^{-/-}$ mice administered Ad-GFP or Ad-GPAT1. *B*, densitometric quantification of phosphorylation of IRS and Akt after normalization to GAPDH and adjustment for GPAT1 expression using ANCOVA. *C*, primary hepatocytes were isolated from *Them2*$^{+/+}$ and *Them2*$^{-/-}$ mice and treated with adenovirus to induce GPAT1 overexpression. Shown are representative immunoblots of insulin-induced phosphorylation of Akt at Thr-308 and Ser-473 in primary hepatocytes from *Them2*$^{+/+}$ and *Them2*$^{-/-}$ mice treated with Ad-GFP or Ad-GPAT1 adenovirus. *D*, GPAT1-specific (detecting the FLAG tag in the construct) protein expression and GPAT1-specific activity (nmol/min/mg) in primary hepatocytes from *Them2*$^{+/+}$ and *Them2*$^{-/-}$ mice upon treatment with Ad-GFP and Ad-GPAT1 constructs ($n = 3$ independent experiments). *E*, quantitative levels of phosphorylated (Thr-308 and Ser-473) Akt per total Akt in Ad-GPAT1–treated hepatocytes relative to the levels in Ad-GFP–treated hepatocytes of each genotype ($n = 3$ independent experiments). Values are presented as mean ± S.E. (*error bars*). Differences in *B* and *E* were assessed by Student's *t* test. #, $p < 0.05$, *Them2*$^{+/+}$ *versus Them2*$^{-/-}$. Differences in *D* were detected by post hoc testing following significant two-way ANOVA. *, $p < 0.05$, GFP *versus* GPAT1.

long-chain fatty acyl-CoAs provides a measure of molecular selectivity in producing long-chain fatty acids (14). In cultured mouse hepatocytes under simulated conditions of fasting, Them2 promotes fatty acid oxidation, apparently by generating FFA, which are re-esterified to provide fatty acyl-CoAs for CPT1-mediated uptake into mitochondria (15). Under these conditions, increased rates of fatty acid oxidation support gluconeogenesis.

GPAT1 plays a central role in the hepatocellular trafficking of fatty acids at the mitochondrion, competing with CPT1a for long-chain fatty acyl-CoAs to generate glycerolipids (4). When GPAT1 activity is low, fatty acid oxidation rates are increased.

Figure 3. Genetic ablation of Them2 protects against GPAT1-induced glucose intolerance. *A–C*, GTTs ($n = 7–10$/group) (*A*), ITTs ($n = 5–6$/group) (*B*), and PTTs (*C*) ($n = 4$/group). Bar plots provide the AUC values. *D*, mRNA expression of genes that regulate glucose metabolism ($n = 7–10$/group). *E*, representative immunoblot analysis of PKCε in total and cytosolic liver membrane fractionations. E-cadherin and GAPDH were used as loading controls for membrane and cytosolic fractions, respectively. Bar plots provide densitometric quantification of PKCε translocation relative to control for each genotype ($n = 5–6$/group). *F*, total hepatic DAG concentrations, as well as relative distribution of DAG grouped according to degree of fatty acid unsaturation ($n = 7–9$/group). Values are presented as mean ± S.E. (*error bars*). Differences in plasma glucose concentrations during tolerance tests were detected by Student's *t* test. *, $p < 0.05$, GFP *versus* GPAT1. Otherwise, differences were detected by the post hoc testing following two-way ANOVA. *, $p < 0.05$, GFP *versus* GPAT1; #, $p < 0.05$, *Them2*$^{+/+}$ *versus Them2*$^{-/-}$.

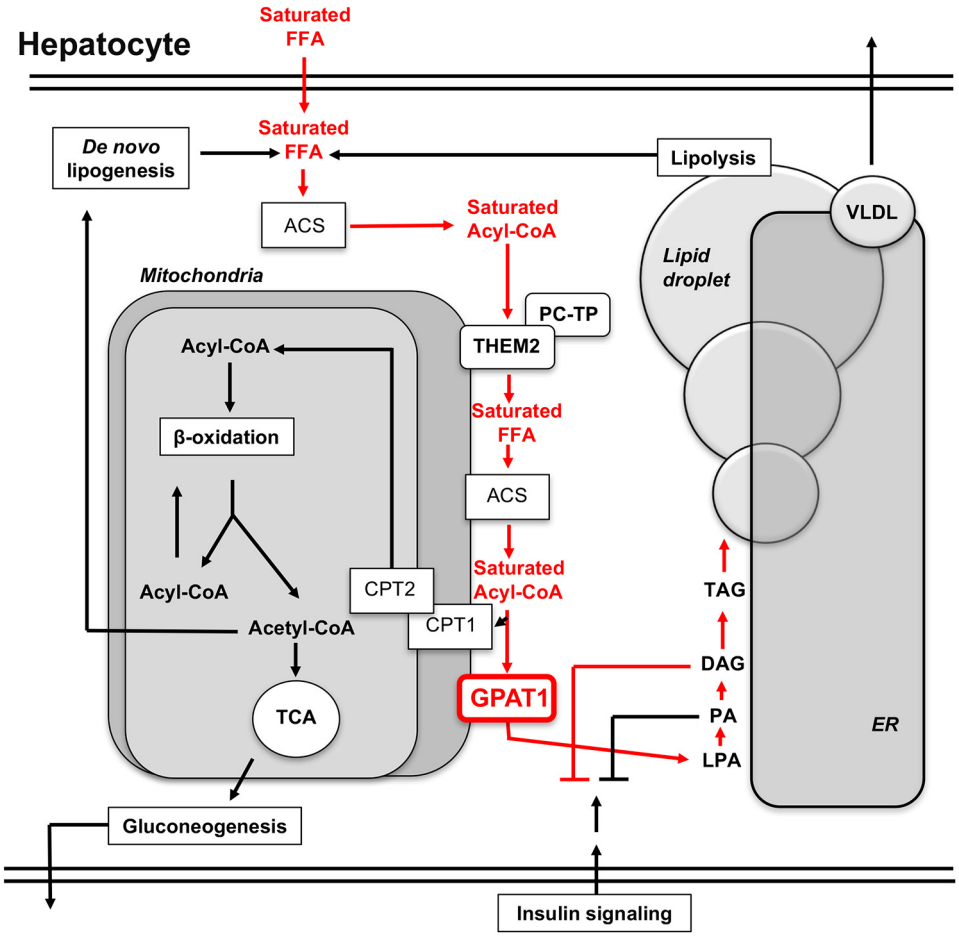

Figure 5. *Schematic model* for the contribution of Them2 to hepatic insulin resistance due to GPAT1 overexpression. FFA are taken up from the plasma, produced by *de novo* lipogenesis, or released by lipolysis. These are converted to fatty acyl-CoAs by various ACSs within the hepatocyte. At the mitochondrial membrane, a fraction of acyl-CoA thioesters is hydrolyzed into FFA by the action of Them2. These FFA become substrates for the mitochondria-associated ACSL1, producing newly synthesized fatty acyl-CoAs that are available for fatty acid oxidation within the mitochondria upon CPT1-mediated uptake. Alternatively, acyl-CoAs may enter the glycerolipid synthetic pathways, which is determined by the activity of GPAT1. Following GPAT1 overexpression, as portrayed by *red type*, Them2 preferentially traffics a fraction of saturated FFA molecules derived from plasma into the glycerolipid synthetic pathway (*red arrows*), leading to the relative enrichment of DAG containing saturated fatty acids, which promote insulin resistance. Because hepatic steatosis is observed even in the absence of Them2, the majority of the fatty acid flux into the glycerolipid pathway occurs through a distinct metabolic pathway. *LPA*, lysophosphatidic acid; *TCA*, tricarboxylic acid; *VLDL*, very low density lipoprotein.

With overnutrition, SREBP1c and ChREBP up-regulate GPAT1, which diverts fatty acids into TAG. The hepatic overexpression of GPAT1 is sufficient to promote hepatic steatosis in chow-fed rats and C57BL/6 mice (6, 8), and the same was observed in the current studies using FVB/NJ mice. The increase in hepatic TAG content was equally robust in *Them2*$^{-/-}$ mice, suggesting that the overexpressed GPAT1 recruits most fatty acid molecules from an alternative source than those that are re-esterified to CoA after hydrolysis by Them2. Unlike in the prior studies (6, 8), FVB/NJ mice did not exhibit increased plasma FFA or TAG concentrations, which, instead, tended to decline. The decrease in plasma FFA concentrations, when taken together with down-regulation of lipogenic genes, suggests that plasma was an important source of FFA for glycerolipid biosynthesis under conditions of forced hepatic GPAT1 overexpression in FVB/NJ mice.

Notwithstanding the inability of Them2 ablation to mitigate GPAT1-mediated hepatic steatosis, *Them2*$^{-/-}$ mice exhibited improved glucose tolerance. The lack of changes in systemic insulin responsiveness is in keeping with the absence of changes in lean and fat mass. Instead, the improvements in glucose tolerance could be attributed to preserved hepatic insulin sensitivity mass in response to hepatic GPAT1 overexpression. This was evidenced by decreased membrane translocation of PKCϵ and more robust Akt phosphorylation at Thr-308 in livers and isolated hepatocytes of *Them2*$^{-/-}$ mice. Although we did not observe differences in insulin signaling following insulin administration *in vivo*, this was not unexpected; we did not observe differences in plasma glucose concentrations during ITTs, which reflect the suppression of hepatic glucose as well as the stimulation of glucose disposal. In addition, our experiments in primary hepatocytes demonstrate that relative reductions in Akt phosphorylation can be captured at insulin concentrations in the physiological range, but not at the high insulin concentrations used for *in vivo* studies. This most likely explains the differences observed in GTTs, which occur in response to physiological increases in plasma insulin concentrations.

Prior studies in mouse hepatocytes have demonstrated reduced activity of mTORC2 to be a major driver of insulin resistance (9, 10). Although DAG and PA were increased by

GPAT1 overexpression, 16:0–16:0 PA specifically promoted disassembly of the mTOR/Rictor complex and thereby reduced phosphorylation of Akt at Ser-473 (10). This finding was supported by the demonstration that enzymatic manipulation of the hepatocellular contents of PA, but not DAG, was sufficient to control insulin responsiveness (9). However, under the current experimental conditions that include the use of FVB/NJ mice, we found that Them2 expression influenced neither phosphorylation of Akt at Ser-437 (24) nor the activity of mTORC2. Instead, we observed reduced Akt phosphorylation at Thr-308 when GPAT1 was overexpressed in the presence of Them2. This indicates impaired insulin signaling attributable to PKCϵ-mediated phosphorylation of the insulin receptor kinase (21). In this connection, total and cytosolic saturated DAG species are associated with hepatic insulin resistance in the setting of GPAT1 overexpression in rats (8) and in human NAFLD (22), respectively.

In the setting of overnutrition, we have demonstrated that Them2 promotes incorporation of saturated fatty acids into membrane phospholipids, leading to leakage of calcium from the ER lumen into the cytosol (16). The reduction in calcium leads to the activation of ER stress pathways that contribute to hepatic insulin resistance, whereas excess cytosolic calcium promotes glucose production through the activation of CaMKII. Although the current study did not demonstrate a statistically significant decrease in the steady-state concentrations of saturated DAG in livers of *Them2*$^{-/-}$ mice, the observed reductions in PKCϵ activation and Akt phosphorylation at Thr-308 together implicate a role for Them2 in the biosynthesis of the saturated DAG molecular species that suppress insulin signaling (22).

Our current findings support a metabolic function of Them2 in the hepatocellular trafficking of saturated fatty acids into the glycerolipid biosynthetic pathway (Fig. 5). A mechanism whereby Them2 promotes the formation of DAG species that suppress insulin signaling confirms and extends our prior demonstration that this enzyme mediates the incorporation of saturated fatty acids into ER membrane phospholipids, thereby promoting ER stress (16). Considering the distinct contributions of saturated DAG and ER stress to insulin resistance and glucose intolerance, the activity of Them2 could represent an attractive target in the management of obesity-related metabolic disorders, including NAFLD and type 2 diabetes.

Experimental procedures

Recombinant adenoviruses

Ad-GPAT1, a recombinant adenovirus designed to express C-terminal FLAG-tagged GPAT1 under the control of a cytomegalovirus promoter (4), was amplified by ViraQuest (North Liberty, IA). An Ad-GFP adenovirus was used as the control (25).

Animal experiments

Them2$^{-/-}$ mice, back-crossed 20 generations to an FVB/NJ genetic background (17, 26), were maintained in a 12-h light-dark cycle barrier facility with free access to drinking water and standard chow (PicoLab Rodent Diet 20, 5053, LabDiets, St. Louis, MO). *Them2*$^{+/+}$ mice were purchased as WT FVB/NJ mice from the Jackson Laboratory (Bar Harbor, ME) and were allowed to acclimate for 2 weeks prior to experiments.

Weight matched 10-week-old male mice were administered 2.0×10^9 pfu of recombinant GPAT1 or GFP adenovirus by retro-orbital injection under isoflurane anesthesia. Mice were then continued on chow diet for the duration of experiments. After a 4-h fast, mice were sacrificed by cardiac puncture under isoflurane anesthesia on day 12. Blood was collected into EDTA-containing microtubes, and plasma was harvested after centrifugation at 4,000 × *g* for 20 min at 4 °C. To assess insulin signaling *in vivo*, on day 13, mice were administered 10 milliunits of insulin/g of body weight or an equal volume of PBS intraperitoneally following a 6-h fast and sacrificed 10 min later (27). Tissues were snap-frozen in liquid nitrogen. Prior to analysis, samples were stored at −80 °C. Animal protocols for treatment, anesthesia, and euthanasia were approved by the Institutional Animal Care and Use Committee of Weill Cornell Medical College.

Body composition

After a 2-h morning fast, mouse lean and fat mass compositions were determined by NMR spectroscopy (EchoMRI 3-in-1 Body Composition Analyzer, Houston, TX).

Glucose, insulin, and pyruvate tolerance tests

GTTs and ITTs were performed after a 4-h morning fast, whereas PTTs were performed after a 16-h fast. For GTTs, tail vein blood samples were collected prior to, at 15 min after, and then at 30-min intervals up to 150 min after intraperitoneal administration of 2 mg/g body weight glucose (diluted in PBS). For ITTs, baseline blood samples were obtained prior to intraperitoneal administration of 0.75 milliunits/g insulin. Blood samples were collected at 15-min intervals up to 90 min. For PTTs, blood samples were collected prior to, 15 min after, and then every 30 min up to 180 min after intraperitoneal administration of 2 mg/g body weight of pyruvate. Blood glucose concentrations were determined using a GE100 blood glucose–monitoring system (GE Diabetes, Taichung, Taiwan).

Hepatocyte isolation and culture

Hepatocytes were isolated and cultured as described (15) with minor modifications. Briefly, mice were anesthetized by IP administration of a mixture of 100 mg/kg ketamine (Ketaset, Pfizer, New York, NY), 10 mg/kg xylazine (AnaSed, Lloyd Laboratories, Malolos, Philippines), and 3 mg/kg acepromazine (Vedco, Saint Joseph, MO). The superior inferior vena cava was clamped, and the inferior vena cava was cannulated. The liver was perfused with Liver Perfusion Medium (Gibco, Thermo Fisher Scientific) and with Liver Digestion Medium (Gibco, Thermo Fisher Scientific) using the portal vein as the exit route. The liver was then removed and placed in a dish containing ice-cold Hepatocyte Wash Medium (Gibco, Thermo Fisher Scientific). The liver capsule was opened, and hepatocytes were carefully harvested. The cell suspension was then passed through a 70-μm cell strainer into cold Hepatocyte Wash Medium and pelleted by centrifugation at 40 × *g* for 4 min at 4 °C. The cell pellet was carefully resuspended and applied to a mixture of 90% Percoll (Sigma-Aldrich) and 10% 10× HBSS

(Sigma-Aldrich). Viable hepatocytes were isolated by centrifugation at 150 × *g* for 10 min at 4 °C. Hepatocytes were washed once in wash medium and then plated in 6-well plates at a density of 5.0×10^5 cells/well in William's E medium supplemented with 10% FBS, 1% penicillin/streptomycin, and 2 mM L-glutamine. Cells were allowed to adhere for 3–4 h, after which the medium was replaced with serum-free medium containing GPAT1 or GFP adenovirus at a multiplicity of infection of 10 for 16–18 h. For insulin-signaling studies, cells were treated with insulin for 10 min before harvesting in cold buffer containaing 50 mM Tris-HCl, pH 7.5, 150 mM NaCl, 2 mM EDTA, 0.35% Nonidet P-40, 0.5% sodium deoxycholate.

GPAT activity

Activities of GPAT enzymes were determined as described (4). Briefly, samples of frozen liver tissue or cultured hepatocytes were homogenized in ice-cold Medium I (250 mM sucrose, 10 mM Tris (pH 7.4), 1 mM EDTA, and freshly added DTT up to 1 mM) using a motor-driven, prechilled glass-Teflon Dounce homogenizer. Membrane fractions were pelleted by ultracentrifugation at 100,000 × *g* for 1 h at 4 °C. Pellets were resuspended to homogeneity in Medium I using a Dounce homogenizer, aliquoted, and stored at −80 °C. GPAT activity was measured according to the rate of conversion of the substrates glycerol 3-phosphate and palmitoyl-CoA to 1-palmitoyl lysophosphatidic acid. The reaction was initiated by the addition of membrane fractions (7.5–10 μg of protein) to a final reaction mixture of 200 μl containing 76 mM Tris-HCl (pH 7.5), 4 mM $MgCl_2$, 8 mM NaF, 1 mg/ml fatty acid–free BSA, 1 mM DTT, 82 μM palmitoyl-CoA (Sigma-Aldrich), 800 μM glycerol 3-phosphate, 3 μCi of [1,2,3-^{3}H]glycerol-3-phosphate (60 Ci/mmol, American Radiolabeled Chemicals, Saint Louis, MO) per reaction. To determine the contribution of GPAT1 to the total GPAT activity, membrane samples were incubated on ice for 15 min in the presence of 2 mM NEM (which inhibits other GPAT isoforms) (Sigma-Aldrich) before initiating the reaction. Reactions were carried out for 10-min periods at room temperature, reaction products were extracted into chloroform and 1% perchloric acid (28), and the radioactivity present in the organic phase was determined by scintillation counting (Beckman LS 6000 scintillation counter, PerkinElmer Life Sciences).

Acyl-CoA thioesterase activity

Acyl-CoA thioesterase activity of liver homogenates was measured as described previously (17). Briefly, frozen tissue samples were homogenized in 20 mM Tris-HCl (pH 7.4), 137 mM NaCl, 1 mM EDTA, and 10% glycerol and then briefly sonicated and centrifuged at 16,000 × *g* at 4 °C for 20 min. Supernatants were used for thioesterase activity measurements using myristoyl-CoA (Sigma-Aldrich) as a substrate. The assay was carried out in buffer containing 50 mM KCl, 10 mM HEPES (pH 7.5), and 0.3 mM 5,5′-dithiobis(2-nitrobenzoic acid) (DTNB; Molecular Probes, Thermo Fisher Scientific). Free CoASH generated due to acyl-CoA thioesterase activity was detected by absorbance at 412 nm following its reaction with DTNB. Assays were carried out in a 96-well format, with time-dependent A_{412} measured using a SpectraMax5 Microplate Reader (Molecular Devices, Sunnyvale, CA). Thioesterase activity was calculated as the initial rate of CoASH produced per mg of total protein using $E_{412} = 13.6\ \text{mM}^{-1}\ \text{cm}^{-1}$ for DTNB. Values of apparent K_m and apparent V_{max} were determined by fitting values of initial reaction rates as functions of substrate concentration to the Michealis–Menten equation using Prism version 7 (GraphPad Software Inc., La Jolla, CA) (29).

PKCε translocation

Translocation of PKCε to the plasma membrane was determined essentially as described (30). Briefly, frozen liver samples were homogenized with a Polytron homogenizer in ice-cold Buffer I (250 mM sucrose, 20 mM Tris-HCl, pH 7.4, 1 mM EDTA, 0.25 mM EGTA), supplemented with cOmplete protease inhibitor mixture and PhosphoSTOP phosphatase inhibitor mixture tablets (Roche, Basel, Switzerland). Homogenates were then centrifuged at 400 × *g* for 15 min at 4 °C, and the supernatants were then further centrifuged at 100,000 × *g* for 1 h at 4 °C. Supernatants were collected and designated as cytosolic fraction, and the membrane pellet was dissolved in Buffer I and further diluted to a 1:1 ratio with Buffer II (20 mM Tris-HCl, pH 7.4, 1 mM EDTA, 0.25 mM EGTA, and 2% Triton X-100), which was supplemented with cOmplete protease inhibitor mixture and PhosphoSTOP phosphatase inhibitor mixture tablets (Roche). Membranes were further solubilized by sonication and centrifuged at 10,000 × *g* for 10 min at 4 °C, and then supernatants were collected and frozen until further use. Equal amounts of cytosolic and membrane fractions (40 μg of total protein/sample) were then denatured using Laemmli buffer and heat, separated by 9% SDS-PAGE, and subjected to immunoblot analysis.

Analytical measurements

Lipids were extracted from liver tissue (31) and dissolved in 3% Triton X-100. Concentrations of cholesterol, TAG, FFA, and phospholipids were measured enzymatically in total liver lipid extracts and plasma (Wako Diagnostics). Plasma activities of ALT and AST were analyzed using colorimetric kits (Stanbio, Boerne, TX).

Histology

Livers were fixed in 4% paraformaldehyde for ~24 h and then rinsed and stored in PBS until embedded in paraffin and cut into 4-μm sections. Tissue sections were mounted on glass slides and stained with hematoxylin and eosin. Images were captured using an Axio Imager M1 microscope with an AxioCam HR camera (Carl Zeiss Inc., Thornwood, NY).

DAG measurements

Hepatic DAGs were extracted from liver homogenates using 25% ethyl acetate/isooctane (32) and derivatized as 2,4-difluorophenyl urethanes (33). Concentrations of DAGs were then determined by normal phase LC-MS/MS analysis (33) using an AB Sciex 4000 QTRAP linear ion trap quadrupole mass spectrometer (Thornhill, Ontario, Canada) at the Mass Spectrometry Lipidomics Core Facility (University of Colorado, Aurora, CO).

Quantitative PCR

Following homogenization of liver samples in TRIzol (Thermo Fisher Scientific) using a TissueLyser II bead mill (Qiagen Inc., Germantown, MD), total RNA was isolated from samples, according to the manufacturer's protocol. Total RNA concentration was measured using a NanoDrop spectrophotometer (NanoDrop 1000, NanoDrop Technologies), and complementary DNA was synthesized of 500 ng of total RNA using High Capacity cDNA (Applied Biosystems, Thermo Fisher Scientific). Quantitative PCRs were performed with specific primers for selected genes using LightCycler FastStart DNA Master^{plus} SYBR Green I (Roche) in a LightCycler 480II system (Roche). Primer sequences are available upon request. Relative gene expression was calculated using the $2^{-\Delta\Delta Ct}$ method using *Rlp32* as the reference gene.

Protein expression

Tissues and cells were homogenized in buffer containing 50 mM Tris-HCl, pH 7.5, 150 mM NaCl, 2 mM EDTA, 0.35% Nonidet P-40, 0.5% sodium deoxycholate plus cOmplete protease inhibitor mixture and PhosSTOP phosphatase inhibitor mixture tablets (Roche). After a 30-min incubation at 4 °C, homogenates were centrifuged at 12,000 × *g* for 20 min at 4 °C, and the supernatants were used for immunoblotting. Protein concentrations were determined by the Bradford assay (34). After denaturation at 95 °C in Laemmli buffer, proteins were separated by SDS-PAGE electrophoresis and transferred to nitrocellulose membrane by electrophoresis using a Trans-Blot SD semi-dry transfer cell (Bio-Rad). Membranes were blocked in 2% milk powder (or in 2% BSA for phosphoproteins) in 1× TST. Antibodies used were as follows: anti-FLAG (Sigma-Aldrich); anti-GPAM (Abcam, Cambridge, UK); anti-THEM2 (12); anti-GFP (Abcam); anti-GAPDH (Abcam); anti-PKCϵ (Santa Cruz Biotechnology, Inc., Santa Cruz, CA); anti-E-cadherin (BD Biosciences); anti-pan-Akt, anti-phospho-Akt(Ser-473), anti-phospho-Akt(Thr-308), anti-phospho-IRS1, and anti-IRS1 (Cell Signaling Technology, Beverly, MA); and anti-β-actin (Sigma). Densitometry was performed using Image Lab software (Bio-Rad Laboratories) or ImageJ (National Institutes of Health).

mTORC2 activity

An mTORC activity assay was performed as described (26). Total liver homogenates were prepared in lysis buffer (40 mM Hepes, pH 7.5, 120 mM NaCl, 1 mM EDTA, 0.3% CHAPS, 50 mM NaF), supplemented with cOmplete protease inhibitor mixture and PhosphoSTOP phosphatase inhibitor mixture tablets (Roche) using a TissueLyser II (Qiagen). Tissue lysates were diluted to 1.5 μg/ml and used for Rictor immunoprecipitation by anti-Rictor (Bethyl Laboratories, Montgomery, TX), with anti-rabbit antisera as a control. Samples were incubated under rotation for 1.5 h at 4 °C. Protein A/G–agarose (MBL International Corp., Woburn, MA) was then added, and samples were further incubated under rotation for 1.5 h at 4 °C. Pellets were washed three times with tissue lysis buffer and further washed three times in mTORC2 reaction buffer (25 mM HEPES, pH 7.5, 2 mM $MgCl_2$, 0.1 M KOAc). Pellets were then dissolved in the same buffer and used for the mTORC2 assay. Briefly, ATP was added to a final concentration of 500 μM to the immunoprecipitate, and the mixture was incubated for 2 min at 32 °C. The reaction was initiated by the addition of 500 ng of recombinant nonphosphorylated Akt1 (SignalChem, Richmond, Canada) and was terminated after 20 min by placing the samples on ice following the addition of Laemmli buffer to the samples. Immunoblot analyses were then performed.

Statistics

Results are presented as mean ± S.E. Student's *t* test was used to compare means between genotypes or treatments. Differences were considered significant for $p < 0.05$. Two-way ANOVA followed by Tukey's multiple-comparison test was used to determine significance across genotypes and treatments. When quantifying phosphorylation of signaling proteins in response to insulin, ANCOVA was used to adjust for unequal hepatic expression levels of GPAT1.

Author contributions—V. T., A. M., R. A. C., and D. E. C. conceptualization; V. T., A. M., M. A.-B., and D. E. C. data curation; V. T., A. M., and M. A.-B. investigation; V. T., M. A.-B., and D. E. C. methodology; V. T., M. A.-B., and D. E. C. writing-original draft; V. T., A. M., M. A.-B., R. A. C., and D. E. C. writing-review and editing; R. A. C. and D. E. C. resources; D. E. C. formal analysis; D. E. C. supervision; D. E. C. project administration.

References

1. Younossi, Z. M., Koenig, A. B., Abdelatif, D., Fazel, Y., Henry, L., and Wymer, M. (2016) Global epidemiology of nonalcoholic fatty liver disease: meta-analytic assessment of prevalence, incidence, and outcomes. *Hepatology* **64,** 73–84 CrossRef Medline
2. Petersen, M. C., and Shulman, G. I. (2017) Roles of diacylglycerols and ceramides in hepatic insulin resistance. *Trends Pharmacol. Sci.* **38,** 649–665 CrossRef Medline
3. Cooper, D. E., Young, P. A., Klett, E. L., and Coleman, R. A. (2015) Physiological consequences of compartmentalized acyl-CoA metabolism. *J. Biol. Chem.* **290,** 20023–20031 CrossRef Medline
4. Lewin, T. M., Wang, S., Nagle, C. A., Van Horn, C. G., and Coleman, R. A. (2005) Mitochondrial glycerol-3-phosphate acyltransferase-1 directs the metabolic fate of exogenous fatty acids in hepatocytes. *Am. J. Physiol. Endocrinol. Metab.* **288,** E835–E844 CrossRef Medline
5. Lindén, D., William-Olsson, L., Rhedin, M., Asztély, A. K., Clapham, J. C., and Schreyer, S. (2004) Overexpression of mitochondrial GPAT in rat hepatocytes leads to decreased fatty acid oxidation and increased glycerolipid biosynthesis. *J. Lipid Res.* **45,** 1279–1288 CrossRef Medline
6. Lindén, D., William-Olsson, L., Ahnmark, A., Ekroos, K., Hallberg, C., Sjögren, H. P., Becker, B., Svensson, L., Clapham, J. C., Oscarsson, J., and Schreyer, S. (2006) Liver-directed overexpression of mitochondrial glycerol-3-phosphate acyltransferase results in hepatic steatosis, increased triacylglycerol secretion and reduced fatty acid oxidation. *FASEB J.* **20,** 434–443 CrossRef Medline
7. Hammond, L. E., Neschen, S., Romanelli, A. J., Cline, G. W., Ilkayeva, O. R., Shulman, G. I., Muoio, D. M., and Coleman, R. A. (2005) Mitochondrial glycerol-3-phosphate acyltransferase-1 is essential in liver for the metabolism of excess acyl-CoAs. *J. Biol. Chem.* **280,** 25629–25636 CrossRef Medline
8. Nagle, C. A., An, J., Shiota, M., Torres, T. P., Cline, G. W., Liu, Z. X., Wang, S., Catlin, R. L., Shulman, G. I., Newgard, C. B., and Coleman, R. A. (2007) Hepatic overexpression of glycerol-*sn*-3-phosphate acyltransferase 1 in rats causes insulin resistance. *J. Biol. Chem.* **282,** 14807–14815 CrossRef Medline
9. Zhang, C., Hwarng, G., Cooper, D. E., Grevengoed, T. J., Eaton, J. M., Natarajan, V., Harris, T. E., and Coleman, R. A. (2015) Inhibited insulin

signaling in mouse hepatocytes is associated with increased phosphatidic acid but not diacylglycerol. *J. Biol. Chem.* **290,** 3519–3528 CrossRef Medline

10. Zhang, C., Wendel, A. A., Keogh, M. R., Harris, T. E., Chen, J., and Coleman, R. A. (2012) Glycerolipid signals alter mTOR complex 2 (mTORC2) to diminish insulin signaling. *Proc. Natl. Acad. Sci. U.S.A.* **109,** 1667–1672 CrossRef Medline
11. Neschen, S., Morino, K., Hammond, L. E., Zhang, D., Liu, Z. X., Romanelli, A. J., Cline, G. W., Pongratz, R. L., Zhang, X. M., Choi, C. S., Coleman, R. A., and Shulman, G. I. (2005) Prevention of hepatic steatosis and hepatic insulin resistance in mitochondrial acyl-CoA:glycerol-*sn*-3-phosphate acyltransferase 1 knockout mice. *Cell Metab.* **2,** 55–65 CrossRef Medline
12. Wei, J., Kang, H. W., and Cohen, D. E. (2009) Thioesterase superfamily member 2 (Them2)/acyl-CoA thioesterase 13 (Acot13): a homotetrameric hotdog fold thioesterase with selectivity for long-chain fatty acyl-CoAs. *Biochem. J.* **421,** 311–322 CrossRef Medline
13. Cheng, Z., Song, F., Shan, X., Wei, Z., Wang, Y., Dunaway-Mariano, D., and Gong, W. (2006) Crystal structure of human thioesterase superfamily member 2. *Biochem. Biophys. Res. Commun.* **349,** 172–177 CrossRef Medline
14. Tillander, V., Alexson, S. E. H., and Cohen, D. E. (2017) Deactivating fatty acids: acyl-CoA thioesterase-mediated control of lipid metabolism. *Trends Endocrinol. Metab.* **28,** 473–484 CrossRef Medline
15. Kawano, Y., Ersoy, B. A., Li, Y., Nishiumi, S., Yoshida, M., and Cohen, D. E. (2014) Thioesterase superfamily member 2 (Them2) and phosphatidylcholine transfer protein (PC-TP) interact to promote fatty acid oxidation and control glucose utilization. *Mol. Cell Biol.* **34,** 2396–2408 CrossRef Medline
16. Ersoy, B. A., Maner-Smith, K. M., Li, Y., Alpertunga, I., and Cohen, D. E. (2018) Thioesterase-mediated control of cellular calcium homeostasis enables hepatic ER stress. *J. Clin. Invest.* **128,** 141–156 Medline
17. Kang, H. W., Niepel, M. W., Han, S., Kawano, Y., and Cohen, D. E. (2012) Thioesterase superfamily member 2/acyl-CoA thioesterase 13 (Them2/Acot13) regulates hepatic lipid and glucose metabolism. *FASEB J.* **26,** 2209–2221 CrossRef Medline
18. Monroy, G., Rola, F. H., and Pullman, M. E. (1972) A substrate- and position-specific acylation of *sn*-glycerol 3-phosphate by rat liver mitochondria. *J. Biol. Chem.* **247,** 6884–6894 Medline
19. Coleman, R. A., and Lee, D. P. (2004) Enzymes of triacylglycerol synthesis and their regulation. *Prog. Lipid Res.* **43,** 134–176 CrossRef Medline
20. Neuschwander-Tetri, B. A. (2010) Hepatic lipotoxicity and the pathogenesis of nonalcoholic steatohepatitis: the central role of nontriglyceride fatty acid metabolites. *Hepatology* **52,** 774–788 CrossRef Medline
21. Petersen, M. C., Madiraju, A. K., Gassaway, B. M., Marcel, M., Nasiri, A. R., Butrico, G., Marcucci, M. J., Zhang, D., Abulizi, A., Zhang, X. M., Philbrick, W., Hubbard, S. R., Jurczak, M. J., Samuel, V. T., Rinehart, J., and Shulman, G. I. (2016) Insulin receptor Thr1160 phosphorylation mediates lipid-induced hepatic insulin resistance. *J. Clin. Invest.* **126,** 4361–4371 CrossRef Medline
22. Ter Horst, K. W., Gilijamse, P. W., Versteeg, R. I., Ackermans, M. T., Nederveen, A. J., la Fleur, S. E., Romijn, J. A., Nieuwdorp, M., Zhang, D., Samuel, V. T., Vatner, D. F., Petersen, K. F., Shulman, G. I., and Serlie, M. J. (2017) Hepatic diacylglycerol-associated protein kinase Cε translocation links hepatic steatosis to hepatic insulin resistance in humans. *Cell Rep.* **19,** 1997–2004 CrossRef Medline
23. Kang, H. W., Ozdemir, C., Kawano, Y., LeClair, K. B., Vernochet, C., Kahn, C. R., Hagen, S. J., and Cohen, D. E. (2013) Thioesterase superfamily member 2/acyl-CoA thioesterase 13 (Them2/Acot13) regulates adaptive thermogenesis in mice. *J. Biol. Chem.* **288,** 33376–33386 CrossRef Medline
24. Sarbassov, D. D., Guertin, D. A., Ali, S. M., and Sabatini, D. M. (2005) Phosphorylation and regulation of Akt/PKB by the rictor-mTOR complex. *Science* **307,** 1098–1101 CrossRef Medline
25. Okada, K., LeClair, K. B., Zhang, Y., Li, Y., Ozdemir, C., Krisko, T. I., Hagen, S. J., Betensky, R. A., Banks, A. S., and Cohen, D. E. (2016) Thioesterase superfamily member 1 suppresses cold thermogenesis by limiting the oxidation of lipid droplet-derived fatty acids in brown adipose tissue. *Mol. Metab.* **5,** 340–351 CrossRef Medline
26. Ersoy, B. A., Tarun, A., D'Aquino, K., Hancer, N. J., Ukomadu, C., White, M. F., Michel, T., Manning, B. D., and Cohen, D. E. (2013) Phosphatidylcholine transfer protein interacts with thioesterase superfamily member 2 to attenuate insulin signaling. *Sci. Signal.* **6,** ra64 Medline
27. Agouni, A., Owen, C., Czopek, A., Mody, N., and Delibegovic, M. (2010) *In vivo* differential effects of fasting, re-feeding, insulin and insulin stimulation time course on insulin signaling pathway components in peripheral tissues. *Biochem. Biophys. Res. Commun.* **401,** 104–111 CrossRef Medline
28. Schlossman, D. M., and Bell, R. M. (1976) Triacylglycerol synthesis in isolated fat cells: evidence that the *sn*-glycerol-3-phosphate and dihydroxyacetone phosphate acyltransferase activities are dual catalytic functions of a single microsomal enzyme. *J. Biol. Chem.* **251,** 5738–5744 Medline
29. Han, S., and Cohen, D. E. (2012) Functional characterization of thioesterase superfamily member 1/acyl-CoA thioesterase 11: implications for metabolic regulation. *J. Lipid Res.* **53,** 2620–2631 CrossRef Medline
30. Qu, X., Seale, J. P., and Donnelly, R. (1999) Tissue and isoform-selective activation of protein kinase C in insulin-resistant obese Zucker rats: effects of feeding. *J. Endocrinol.* **162,** 207–214 CrossRef Medline
31. Folch, J., Lees, M., and Sloane Stanley, G. H. (1957) A simple method for the isolation and purification of total lipides from animal tissues. *J. Biol. Chem.* **226,** 497–509 Medline
32. Hutchins, P. M., Barkley, R. M., and Murphy, R. C. (2008) Separation of cellular nonpolar neutral lipids by normal-phase chromatography and analysis by electrospray ionization mass spectrometry. *J. Lipid Res.* **49,** 804–813 CrossRef Medline
33. Leiker, T. J., Barkley, R. M., and Murphy, R. C. (2011) Analysis of diacylglycerol molecular species in cellular lipid extracts by normal-phase LC-electrospray mass spectrometry. *Int. J. Mass Spectrom.* **305,** 103–109 CrossRef Medline
34. Bradford, M. M. (1976) A rapid and sensitive method for the quantitation of microgram quantities of protein utilizing the principle of protein-dye binding. *Anal. Biochem.* **72,** 248–254 CrossRef Medline